PHYSICAL REVIEW B, VOLUME 64, 020405(R)

Structural and physical properties of double-layered manganites $La_{2-2x}Ca_{1+2x}Mn_2O_7$ with $0.5 \leqslant x \leqslant 1.0$

J. Q. Li, C. Q. Jin, and H. B. Zhao
Institute of Physics, Chinese Academy of Sciences, Beijing 100080, China
(Received 13 March 2001; published 19 June 2001)

Structural and physical properties of the double-layered manganites $La_{2-2x}Ca_{1+2x}Mn_2O_7$ ($0.5 \leqslant x \leqslant 1.0$), prepared under a high pressure of 4.5 GPa, have been systematically investigated. A charge-ordered state has been revealed at low temperatures in the samples with $0.6 \leqslant x \leqslant 0.75$. The $x = 0.6$ material undergoes the charge-ordering transition at ~280 K and, successively, a ferromagnetic (FM) transition at ~160 K with evident colossal magnetoresistance effects under applied magnetic fields. A phase separation resulting from the competition between the charge-ordered state and the FM state is observed in the $x = 0.6$ material below 160 K.

DOI: 10.1103/PhysRevB.64.020405 PACS number(s): 75.30.Kz, 64.70.Rh, 71.38.−k, 75.50.Cc

Manganese oxides with either the simple cubic structure or the layered perovskite structure exhibit extraordinary physical properties,[1–6] such as, the colossal magnetoresistance (CMR) and charge ordering (CO). In order to understand these unusual properties, particular attentions have been paid to the strong correlation among the e_g electrons, the t_{2g} spins, and the cooperative Jahn-Teller effects in this kind of materials.[7–11] In recent literatures, phase separation (PS) and phase competition between the CO and FM states have been discussed on account for the complex magnetic and electronic properties observed in the related systems.[12,13] In this Rapid communication, we report on the investigations of structural and physical properties in the double-layered manganites $La_{2-2x}Ca_{1+2x}Mn_2O_7$ ($0.5 \leqslant x \leqslant 1.0$). A CO modulation, FM properties, and a phase separation have been extensively examined in the $x = 0.6$ sample.

A series of ceramic materials with nominal compositions of $La_{2-2x}Ca_{1+2x}Mn_2O_7$ ($0.5 \leqslant x \leqslant 1.0$) were used in the present investigation. These materials were prepared by mixing up La_2O_3, Ca_2MnO_4, and MnO_2 in the desired proportions, and then fired at around 1000 °C in air for several hours. High-pressure syntheses were carried out at around 1200 °C under a high pressure of 4.5 GPa as reported in Ref. 14. A H-9000NA transmission electron microscope (TEM), equipped with low-temperature sample stages, was used for investigating the microstructural properties of these materials from the room temperature down to ~30 K.

Structural measurements by means of x-ray diffraction and TEM observation have been performed on the samples of $La_{2-2x}Ca_{1+2x}Mn_2O_7$ ($0.5 \leqslant x \leqslant 1.0$), the results indicate that samples with $0.6 \leqslant x \leqslant 1.0$ can be considered as single-phase materials with an average structure of the tetragonal perovskite ($Sr_3Ti_2O_7$-type, $I4/mmm$). However, the sample with $x = 0.5$ is not of single phase, but intergrown with the other impurity phases, such as $La(Ca)MnO_3$ and $CaCO_3$ as observed. Figures 1(a) and 1(b) show the electron-diffraction patterns for the $x = 0.7$ sample, taken along the [100] and [110] zone-axis directions, respectively. All diffraction spots can be well indexed by a bilayered-perovskite unit cell with lattice parameters of $a = b = 0.38$ nm, and $c = 19.92$ nm. In Fig. 1(c), we display the high-resolution image directly showing the atomic structure of the layered $La_{0.6}Ca_{2.4}Mn_2O_7$ crystal. This image, along the [100] zone-axis direction, was obtained from the thin region of a crystal under the defocus value at around the Scherzer defocus (~45 nm). The metal-atom positions are therefore recognizable as dark dots. The atomic layers in the $(La, Ca)_3Mn_2O_7$ phase along the c direction can be clearly read out in this image. Image calculations, based on the proposed structural model,[15,16] was carried out by varying the crystal thickness from 2 to 5 nm and the defocus value from −30 to −60 nm. A calculated image with the defocus value of −0.45 nm and the thickness of 3 nm is superimposed on the image, and appears to be in good agreement with the experimental one. Structural alteration upon the increase of doping levels (x) has been systematically analyzed, a structural distortion has been observed evidently in the samples with $x > 0.85$. This structural distortion could result from a noticeable rotation of the MnO_6 octahedra or some kinds of structural instability.[16] Figure 1(d) shows the electron diffraction pattern taken along the [110]-zone axis direction the $x = 0.9$ sample, the additional rows of reflection spots are typically indicated by arrows. Systemati-

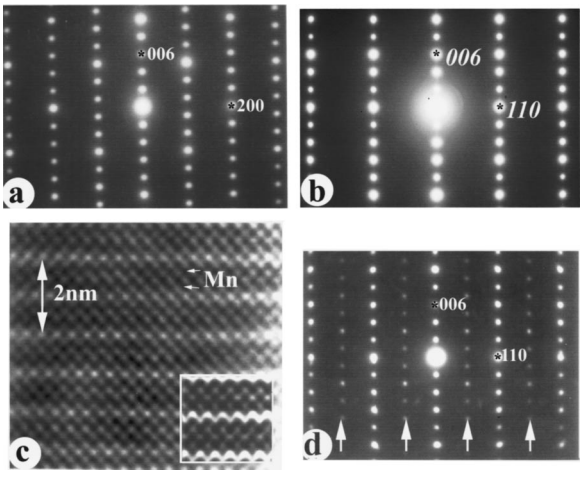

FIG. 1. Structural properties of $La_{2-2x}Ca_{1+2x}Mn_2O_7$. (a), (b) Electron diffraction patterns for $x = 0.7$, taken along the ⟨100⟩ and ⟨110⟩ directions, respectively. (c) High-resolution image showing the atomic layers of the $La(Ca)_3Mn_2O_7$ crystal. (d) Electron diffraction pattern showing the additional reflection spots from a structural distortion in $x = 0.90$.

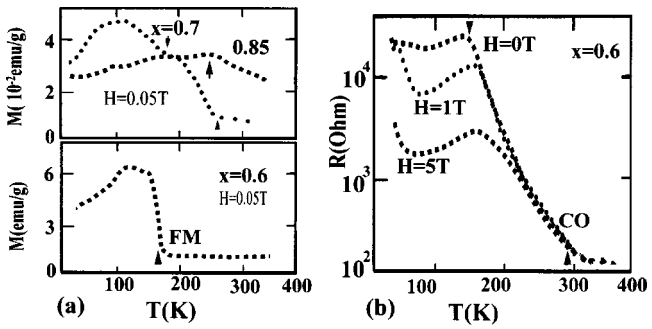

FIG. 2. (a) Temperature dependence of magnetization (upper panel) for 0.85 with an AFM transition at around 250 K, for $x=0.7$ with weak FM properties at low temperatures, and (lower panel) for the $x=0.6$ sample with a FM transition at ~160 K. (b) Temperature dependence of resistivity for $x=0.6$, illustrating the CMR effects under applied magnetic fields at around 160 K. Furthermore, a CO anomaly can be recognized just below 300 K.

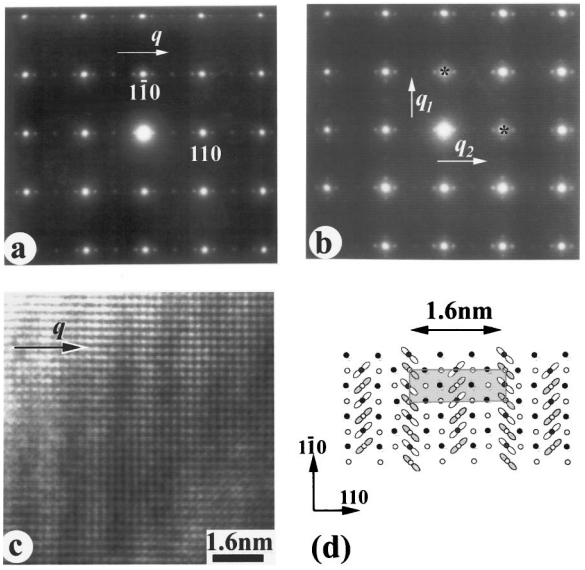

FIG. 3. The CO phenomenon in $La_{2-2x}Ca_{1+2x}Mn_2O_7$ with $0.6 \leqslant x < 0.8$. (a) Electron-diffraction pattern (at ~150 K) showing the CO satellite spots within the a^*-b^* plane. (b) Electron-diffraction pattern showing the presence of 90° CO domain at low temperatures. (c) TEM image clearly exhibiting a CO modulation with a periodicity of 1.6 nm. (d) Schematic representation of the charge/orbital ordered state projection along the ⟨001⟩ direction. In order to simplify the drawing only Mn^{3+} and Mn^{4+} are shown.

cal analysis suggests this structural distortion emerges in all materials within the doping range of $0.85 \leqslant x \leqslant 1.0$. The resultant distorted structure has a pseudotetragonal unit cell with parameters of $a=b=0.542$ nm, and $c=1.94$ nm, and a space group of $Bmbm$ or $Bm2m$ with the reflection conditions of $h+1=2n$ for (hkl), $h+k=2n$ for $(hk0)$, and $h+1=2n$ for $(0kl)$. Recently, similar structural features have been investigated by TEM and interpreted by tilting of the MnO_6 octahedra.[17]

We now go on to discuss the electric transport and magnetic properties of $La_{2-2x}Ca_{1+2x}Mn_2O_7$ $(0.5 \leqslant x \leqslant 1.0)$. In the doping range of $x>0.8$, all samples are found to be insulators without any FM behavior for the whole temperature range from 400 K down to 4 K. An evident alternation of magnetic property is found at ~250 K in connection with a possible antiferromagnetic (AFM) transition.[14] On the other hand, in the doping range of $0.6 \leqslant x \leqslant 0.75$, we have observed apparent FM attributes at low temperatures. Figure 2(a) display the temperature dependence of magnetizations for $x=0.85$,0.7 (upper panel), and 0.6 (lower panel). The $x=0.85$ sample shows an AFM-like transition at around 250 K.[14] The $x=0.7$ sample has relatively complex magnetic properties, first change occurs at ~270 K in association with the appearance of a short-range magnetic order, second is at ~165 K in connection with a FM transition, the similar kind of multimagnetic transitions have been discussed in layered materials.[14,16] The most notable feature revealed in the magnetic measurements is the presence of a FM transition in the $x=0.6$ sample at the temperature of around 160 K.

Figure 2(b) shows the temperature dependence of resistivity for the double-layered manganite $La_{0.8}Ca_{1.2}Mn_2O_7$ ($x=0.6$) under different applied magnetic fields of $H=0$,3, and 5 T. Evident anomalous behaviors occur at around ~160 K originating from the FM transition as shown in Fig. 2(a). The magnetic-field effects on resistivity are small above the FM transition, and, then become apparently larger below 160 K. In the temperature range from ~170 K down to 70 K, evident negative magnetoresistance (MR) effects has been observed. For instance, according to the experimental data for $H=5$ T, we can obtain a MR ratio, as defined by $R(0)/R(H)$, to be ~1200% at 120 K.

Then it is worth noting that there is another anomalous behavior, showing up as a remarkable upturn in resistivity just below 300 K. A systematic analysis suggests it corresponds to a CO transition, and, below this CO critical temperature, the rapid increase of resistivity is due to the freezing of charge carriers on the lattice sites. Direct evidences of the CO states in this double-layered manganese system have been obtained from the low-temperature TEM investigations. Figure 3(a) shows an electron-diffraction pattern taken at ~150 K for $La_{2-2x}Ca_{1+2x}Mn_2O_7$ with $x=0.60$, exhibiting the satellite spots of a CO modulation following with the main reflection spots. This CO modulation (**q**) appears along the ⟨110⟩ direction within the **a***-**b*** plane, the wave vector of the resultant structural modulation can be written as $\mathbf{q}=(1/6,1/6,0)$. The satellite spots are generally very sharp, directly indicating the long-coherent nature (>100 nm) of the CO state in this kind of material. Sometimes, two sets of satellite reflections become visible around each basic Bragg spot as shown in Fig. 3(b), those are considered to originate from twin domains where the CO modulation wave vectors are rotated by 90° with respect to one another.[18,19]

The changes of CO properties along with the nominal hole-density x have been examined at low temperatures. This CO state is found to be visible within the doping levels of $0.6<x<0.80$ at low temperatures, and, furthermore, the CO states in all these samples have the same modulation wave vector, i.e., $\mathbf{q}=(1/6,1/6,0) \sim 1/6d_{110}$ as discussed above. This property is apparently different from the results observed previously in the other manganites, such as $La(Ca)MnO_3$ and

$Pr(Ca)MnO_3$,[7,9] in those systems a linear relationship between the modulation wave vector (q) and the charge-carrier density (x) is commonly observed. For instance, a CO modulation with $\mathbf{q}\sim 1/8d_{110}$ has been evidently observed in the $Pr_{0.25}Ca_{0.75}MnO_3$ ($x=0.75$) sample.

TEM observations of the structural features in association with this CO state have been performed in these samples at low temperatures. Figure 3(c) represents a high-resolution TEM image obtained from the CO material with $x=0.7$ at around 150 K, clearly showing a structural modulation with a periodicity of $L\approx 6d_{110}\approx 1.6$ nm. Following with the ways used previously for explaining the CO modulations in both the cubic and layered perovskite manganites,[7,9,15] we found that the structural model as shown in Fig. 3(d) can be used in principle to explain our experimental results. It should be noted that this model only represents the projection of the CO state along the $\langle 001\rangle$ direction, which contains ordered arrangements of the Mn^{3+} and Mn^{4+} ions accompanied by the $d_z2(Mn^{3+})$ orbital ordering. From this model, the localized d_z2 electrons at low temperatures corresponds to a nominal density of $x\sim 2/3$, the orientational order of the $d_z2(Mn^{3+})$ orbits yields directly a structural modulation with the periodicity of $L=1.6$ nm with in the a-b plane.

Now we go on to discuss the correlation and competition between the CO state and the ferromagnetic state in the materials with $x=0.6$, which first undergoes the CO transition at around 280 K and then the FM transition at round 160 K. Below this FM transition, we have observed clear evidences suggesting the appearance of a phase separation, with which we are mainly concerned in the following discussions.

Figure 4(a) shows two electron-diffraction patterns taken from the $x=0.6$ sample, exhibiting the CO spots above ($\sim$180 K) and below ($\sim$100 K) the FM transition. It can be clearly recognized that the intensity of these CO satellites turns out to be much lower at $\sim$100 K. Figure 4(b) shows the microphotometric density curves demonstrating the evolution of the satellite peaks as observed in the $x=0.6$ sample. Upon cooling from room temperature, the satellite reflections appear just below $\sim$280 K, afterward, their average intensity increases gradually and reaches a maximum at around 170 K. Then, these CO satellite spots become weaker with lowering temperature. Below 100 K, the satellite spots looks notably broader [see Fig. 4(a)], so the coherent length of this CO state becomes short ($<$30 nm); previously, this kind of phase competition between the CO state and the FM state is discussed in the perovskite systems.[12,13] As a result, the phase separation is proposed theoretically and observed experimentally in several typical materials.

TEM observation of the phase separation in present system was performed in the $x=0.6$ sample at low temperatures. Figures 4(c) and 4(d) show the dark-field TEM images of a thin area taken at $\sim$190 and $\sim$120 K, respectively; these images are obtained by using one of the satellite spots following with the (020) main spot. The submicrometer-scale

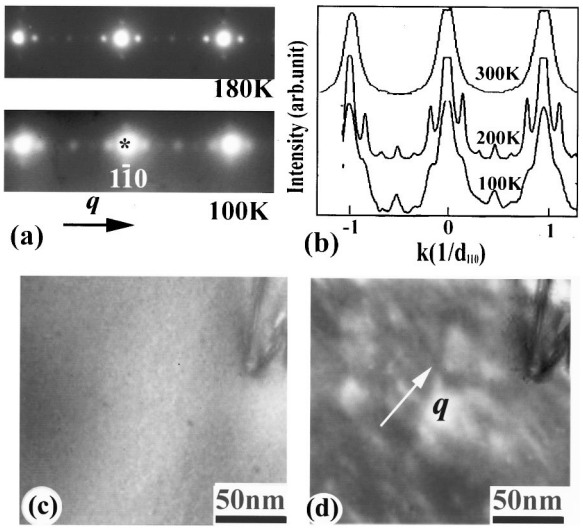

FIG. 4. Phase separation in the $x=0.6$ material. (a) Electron-diffraction patterns showing the changes of CO satellite spots along with the FM transition. (b) Microphotometeric density curves showing the temperature variation of satellite reflections. (c), (d) Dark-field images taken at the temperatures of 190 and 120 K, respectively. The CO domains resulting from the phase separation can be clearly recognized. A dislocation appears at the upper right corners in both images.

CO region with relatively uniform contrast at 190 K undergoes into a state with fine speckled contrasts at 120 K. This kind of contrast evolution has been discussed before in the analyses of charge-order melting in the perovskite manganites, and described as a percolative phase separation.[20] The complex contrast in Fig. 4(d) can be explained directly as the coexistence of charge-ordered bright speckles and charge-disordered dark speckles. Taking into account of the FM transition in the $x=0.6$ material, we can conclude that the charge-disordered speckles are mainly governed by the FM metallic phase.

In conclusion, the bilayered manganites $La_{2-2x}Sr_{1+2x}Mn_2O_7$ with $0.5\leqslant x\leqslant 1.0$ have been synthesized under a high pressure of 4.5 GPa. FM transitions have been observed in the $x=0.6$ sample. A CO state with a periodicity of 1.6 nm appears at low temperatures in the samples with $0.6\leqslant x\leqslant 0.75$. The $x=0.6$ sample undergoes a CO transition at $\sim$280 K and, subsequently, a FM transition at $\sim$160 K with an evident CMR effect under the applied magnetic field of $H=5$ T. A percolative phase separation, along with the competition between the CO phase and the FM phase, has been observed in the $x=0.6$ material.

We would like to thank Professor L. Li and S. L. Jia for their assistance with preparing samples and measuring some physical properties. The work reported here was supported by the ''Hundreds of Talents'' program organized by the Chinese Academy of Sciences, P. R. China, and by the ''Outstanding Youth Fund (C.Q.J.), Grant No. 59725105.

[1] K. Chabara, T. Ohno, M. Kasai, and Y. Kozono, Appl. Phys. Lett. **63**, 1990 (1993).
[2] R. von Helmolt, H. Weckerg, B. Holzapfel, L. Schultz, and K. Samwar, Phys. Rev. Lett. **71**, 2331 (1993).
[3] Y. Tokura, A. Urushibara, and N. Furukawa, J. Phys. Soc. Jpn. **63**, 3931 (1994).
[4] H. Asano, J. Hayakawa, and M. Matsui, Phys. Rev. B **56**, 5395 (1997); R. Ganguly, V. Siruguri, I. K. Gopalakrishnan, and J. V. Yakhmi, Appl. Phys. Lett. **76**, 1956 (2000).
[5] T. Mizokawa and A. Fujimori, Phys. Rev. B **56**, R493 (1997).
[6] T. Kimura, Y. Tomioka, H. Kuwahara, A. Asamitsu, M. Tamura, and Y. Tokura, Science **274**, 1698 (1996).
[7] C. H. Chen, S.-W. Cheong, and A. S. Cooper, Phys. Rev. Lett. **71**, 2461 (1993).
[8] J. M. Tranquada, B. J. Sternlieb, J. D. Axe, Y. Nakamura, and S. Uchida, Nature (London) **375**, 561 (1995).
[9] C. H. Chen and S-W. Cheong, Phys. Rev. Lett. **76**, 4042 (1996).
[10] A. J. Millis, R. Mueller, and B. I. Shraiman, Phys. Rev. B **54**, 5405 (1996).
[11] Q. Yuan and P. Thalmeier, Phys. Rev. Lett. **83**, 3502 (1999).
[12] A. Moreo, S. Yunoki, and E. Dagotto, Science **283**, 2034 (1999).
[13] G. Varelogiannis, Phys. Rev. Lett. **85**, 4172 (2000).
[14] H. B. Zhao and C. Q. Jin, Chinese J. High Pressure Phys. **13**, 33 (1999).
[15] Y. Moritomo, A. Asamitsu, H. Kuwahara, and Y. Tokura, Nature (London) **380**, 141 (1996).
[16] P. D. Battle, M. A. Green, N. S. Laskey, J. E. Millburn, M. J. Rosseinsky, S. P. Sullivan, and J. F. Vente, Chem. Mater. **9**, 1042 (1997).
[17] L. A. Bendersky, R. J. Chen, I. D. Fawcett, and M. Greenblatt, J. Solid State Chem. **157**, 309 (2001).
[18] J. Q. Li, Y. Matsui, T. Kimura, and Y. Tokura, Phys. Rev. B **57**, R3205 (1998).
[19] T. Kamura, R. Kumai, Y. Tokura, J. Q. Li, and Y. Matsui, Phys. Rev. B **58**, 11 081 (1998).
[20] M. Uehara, S. Mori, C. H. Chen, and S.-W. Cheong, Nature (London) **399**, 560 (1999).